Wave-front sensing from defocused images by use of wave-front slopes

Marcos A. van Dam and Richard G. Lane

We describe a novel technique for deriving wave-front aberrations from two defocused intensity measurements. The intensity defines a probability density function, and the method is based on the evolution of the cumulative density function of the intensity with light propagation. In one dimension, the problem is easily solved with a histogram specification procedure, with a linear relationship between the wave-front slope and the difference in the abscissas of the histograms. In two dimensions, the method requires use of a Radon transform. Simulation results demonstrate that good reconstructions can be attained down to 100 photons in each detector. In addition, the method is insensitive to scintillation at the aperture.

OCIS codes: 010.1080, 010.7350.

1. Introduction

A problem of interest in astronomical imaging is to estimate the wave-front aberrations. This estimate can then be used to drive a deformable mirror in an adaptive optics system. A wave-front sensor is a device used to estimate the aberration of a wave front at the optical aperture from measurements of photons. There are four wave-front sensors used in astronomical adaptive optics: the lateral shear interferometer[1]; the Shack–Hartmann[1,2] and pyramid sensors,[3] all of which measure the slope of a wave front; and the curvature sensor, which measures its curvature.[2,4] The wave-front derivatives are then used to reconstruct the wave front.[5]

In this paper we describe a novel wave-front sensing scheme that uses directly the linear relationship obtained from geometrical optics between the slope of the wave front and the displacement of a photon. Another key aspect of this method is the idea that the intensity of the propagated wave front represents a probability density function (PDF) for the probability of photon arrival. As the wave propagates, the aberrations of the wave front can be considered to warp the PDF of photon arrival. Inverting this warping gives us wave-front slope estimates from which the wave-front aberrations can be derived. The total area under the one-dimensional PDF curve remains constant, which models the conservation of flux in the wave-front propagation. The change in the PDF from one detector plane to another can be seen indirectly by the cumulative distribution function (CDF). Diffraction effects are not explicitly included in this model. In this regard, the behavior of this sensor is similar to that of the curvature sensor, where it is known that the effect of diffraction is to limit the spatial resolution of the wave-front sensor.[6,7]

The experimental setup is identical to that of the curvature sensor, where there are two measurement planes at distances $\pm z$ from the aperture.[4] The propagation is usually achieved by one using a converging lens and taking positive and negative defocused images. For analysis, however, it is simpler to imagine that the photons are traveling from one plane to the other through an aperture. The propagation of the photons is assumed to follow the laws of geometrical optics, so the direction of propagation is perpendicular to the wave front. Because geometrical optics is assumed, this technique works even for extended and polychromatic sources.

We show that slope estimates can be obtained directly from what is conventionally considered to be curvature sensing data. Unlike existing wave-front slope sensors, the method presented in this paper measures the wave-front slope without introducing any spatial or temporal modulation. Hartmann sensors, for example, also compare the intensity of two

The authors are with the Department of Electrical and Computer Engineering, University of Canterbury, Private Bag 4800, Christchurch 1, New Zealand. The e-mail address for R. G. Lane is r.lane@elec.canterbury.ac.nz.

Received 14 February 2002; revised manuscript received 19 April 2002.

0003-6935/02/265497-06$15.00/0

symmetrically defocused images, but the light passes first through a pupil mask.[8]

2. Propagation of the Cumulative Distribution Function

Initially, we consider the evolution of the CDF as the wave propagates for the simpler one-dimensional case. The one-dimensional case corresponds to the hypothetical case of a two-dimensional wave front where all the wave-front and intensity variations are in one direction only. As shown in Section 4, the analysis can be extended to the two-dimensional case that is of interest in practice.

Consider an aberrated wave front $W(x, z)$ in one spatial dimension propagating in the z direction. The change in a propagating wave can be modeled by the relationships between the intensity and the wave front found by Teague.[9] The derivative of the intensity $I(x, z)$ with respect to z, $I_z = \partial I/\partial z$, is governed by the irradiance transport equation, which, in one dimension, is

$$I_z = -I_x W_x - I W_{xx}, \tag{1}$$

where subscripts are used to denote partial derivatives. The corresponding change in the wave front is given by the wave-front transport equation:

$$W_z = 1 - \frac{1}{2} W_x^2 + \frac{\lambda^2}{16\pi^2 I} I_{xx} - \frac{\lambda^2}{32\pi^2 I^2} I_x^2, \tag{2}$$

where λ is the wavelength. The terms in λ represent the change in the wave front that is due to diffraction and are neglected in the derivation that follows. There is a minor error in Eq. (5) of Teague's paper: The last term should be $2k^2I^2$.

The CDF at the aperture $z = 0$ is

$$C(x, 0) = \int_{-\infty}^{x} I(x', 0)\mathrm{d}x', \tag{3}$$

where x' is the dummy variable in place of x. We want to find the change in x needed to maintain the CDF at the same value as the wave propagates to distance z. Taking a first-order Taylor-series expansion with respect to x and z of the CDF around the point $(x, 0)$ yields

$$C(x + \epsilon, z) \approx C(x, 0) + \epsilon C_x(x, 0) + z C_z(x, 0). \tag{4}$$

The partial derivatives of $C(x, 0)$ are found when we differentiate Eq. (3) with respect to x,

$$C_x(x, 0) = I(x, 0), \tag{5}$$

and z,

$$C_z(x, 0) = \int_{-\infty}^{x} I_z(x', 0)\mathrm{d}x'. \tag{6}$$

Substituting the irradiance transport equation into Eq. (6) yields

$$\begin{aligned} C_z(x, 0) &= \int_{-\infty}^{x} -I_x(x', 0)W_x(x', 0) \\ &\quad - I(x', 0)W_{xx}(x', 0)\mathrm{d}x' \\ &= -I(x, 0)W_x(x, 0). \end{aligned} \tag{7}$$

We are now able to use Eqs. (5) and (7) to substitute for $C_x(x, 0)$ and $C_z(x, 0)$, respectively, into approximation (4), yielding

$$C(x + \epsilon, z) - C(x, 0) = \epsilon I(x, 0) - z I(x, 0)W_x(x, 0). \tag{8}$$

We define Δx to be the value of ϵ such that $C(x + \epsilon, z) = C(x, 0)$. Therefore, setting the left-hand side of Eq. (8) to zero,

$$0 = \Delta x I(x, 0) - z I(x, 0)W_x(x, 0), \tag{9}$$

yields

$$W_x(x, 0) = \Delta x/z. \tag{10}$$

Now taking the second-order terms of the Taylor-series expansion of the CDF and equating the CDF at $(x + \epsilon, z)$ to the CDF at $(x, 0)$ to obtain Δx, we obtain

$$\begin{aligned} 0 &= \frac{(\Delta x)^2}{2} C_{xx} + z\Delta x C_{xz} + \frac{z^2}{2} C_{zz} \\ &= \frac{(\Delta x)^2}{2} I_x + z\Delta x I_z + \frac{z^2}{2}(-I_z W_x - I W_{xz}), \end{aligned} \tag{11}$$

where, for compactness of notation, brackets are omitted when an expression is evaluated at $(x, 0)$. Neglecting the wavelength-dependent terms of the wave-front transport equation, the wave-front slope changes according to

$$W_{xz} = -W_x W_{xx}. \tag{12}$$

Hence,

$$\begin{aligned} 0 &= \frac{(\Delta x)^2}{2} I_x + z\Delta x(-I_x W_x - I W_{xx}) + \frac{z^2}{2}(-I_z W_x \\ &\quad + I W_x W_{xx}) \\ &= \frac{(\Delta x)^2}{2} I_x + z\Delta x(-I_x W_x - I W_{xx}) + \frac{z^2}{2}[(I_x W_x \\ &\quad + I W_{xx})W_x + I W_x W_{xx}], \end{aligned} \tag{13}$$

which, again, has a solution $W_x = \Delta x/z$. It was verified with MATHEMATICA that the third-, fourth-, and fifth-order Taylor-series expansion also have a solution given by Eq. (10), so the relationship appears to be an exact geometrical optics relationship. This is in contrast with the curvature sensor, where the geometric error in the estimation of the curvature is of the order of z^2.[6]

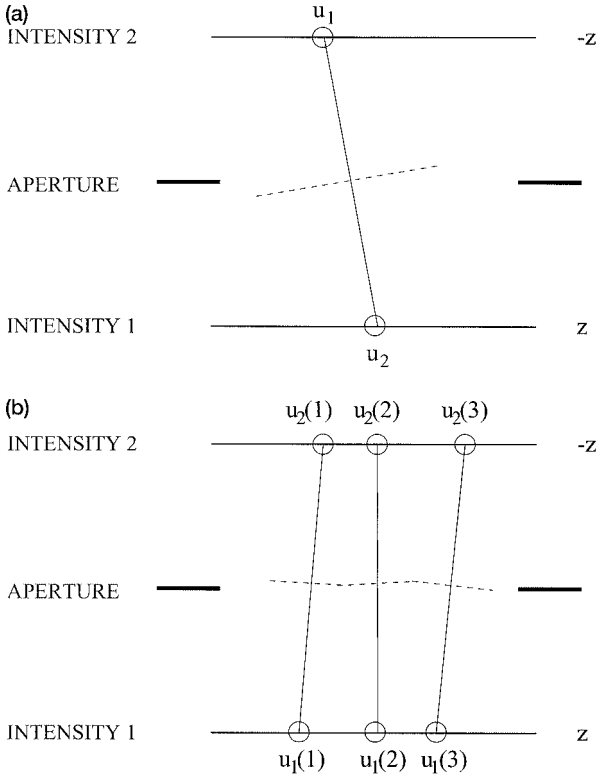

Fig. 1. Estimation of the wave front with (a) one detected photon and (b) three detected photons in each plane.

The algorithm for two detection planes equidistant from the aperture consists of finding points in either plane at which the CDF has the same value. These points are used to define the slope of the wave front at a position in the aperture midway between them.

3. Wave-Front Reconstruction in One Dimension

The wave-front reconstruction algorithm can also be conceived in terms of individual photon detection. A photon is detected in each of the two planes at $x = u_1$ and $x = u_2$, respectively, as shown in Fig. 1(a). To estimate the wave front $W(x)$, it is assumed that a photon travels in a straight line from one plane at $-z$ to the other at z, with the displacement given by the wave-front slope multiplied by the distance between the planes. Then a wave-front slope estimate is obtained at a point halfway between the position of the two photons. If we now consider three photons detected in each plane, as in Fig. 1(b), matching the nth photon in one plane, $u_1(n)$, onto the nth photon of the other, $u_2(n)$, gives the solution with the smallest possible sum of squared distances. This yields the smallest possible sum of squared wave-front slopes.

In a practical implementation, several independent photon events are measured at discrete pixels, and this measurement must be converted to a continuous intensity distribution. The PDF can be modeled as a discontinuous function $f_X(x)$, as shown in Fig. 2. The value of the PDF is the number of photons in a pixel divided by the total number of photons and also by the width of the pixel. This ensures that

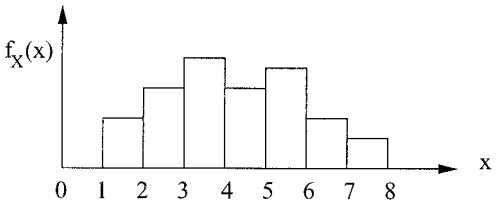

Fig. 2. Model of the PDF. For convenience, the pixels are mapped onto integer values of x.

$$\int_{-\infty}^{\infty} f_X(x)\mathrm{d}x = 1, \tag{14}$$

as required for a PDF. The CDF, $C(x)$, is then found when we integrate the PDF:

$$C(x) = \int_{-\infty}^{x} f_X(x')\mathrm{d}x'. \tag{15}$$

The next step is to match the abscissas (x ordinates) in each of the planes where the CDFs are equal to a sequence of values $s(i)$ between 0 and 1. This procedure is known as histogram specification and is common in image processing.[10] We denote the ordinates where the CDFs are equal to the values of $s(i)$ as $u_1(i)$ and $u_2(i)$, respectively:

$$C_1[u_1(i)] = C_2[u_2(i)] = s(i). \tag{16}$$

Note that values of $s(i)$ that are close to 0 or 1 are dominated by diffraction, and the slope estimates in that region are consequently of lower accuracy. From the points where the constant CDF lines intersect C_1 and C_2, two sets of ordinates, $\mathbf{u}_1$ and $\mathbf{u}_2$, are obtained. Figure 3 plots the two CDFs and the con-

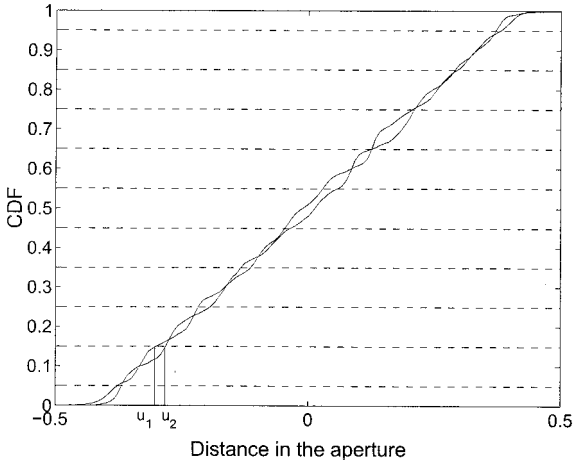

Fig. 3. Normalized CDFs $C_1(x)$ and $C_2(x)$ and the sampling intervals $\mathbf{s} = (0.05, 0.15, 0.25, \ldots, 0.95)$. As an example, the points where each of the curves intersect $s(2) = 0.15$ are marked u_1 and u_2, respectively.

stant CDF lines corresponding to the sampling intervals **s**.

Using the relationship

$$W_x\left[\frac{u_1(i) + u_2(i)}{2}\right] = \frac{u_1(i) - u_2(i)}{2z}, \qquad (17)$$

we obtain a set of slope estimates at approximately regular intervals. The wave front is reconstructed when we integrate the wave-front slopes along the x axis. Any constant of integration can be added to the computed wave front, but this constant term, called the piston, is irrelevant in wave-front sensing.

In the absence of diffraction, this method would give exact wave-front reconstructions, even when there is scintillation at the aperture. For photon-limited data, as z increases, the sensitivity of the sensor improves. However, increased diffraction effects result in a loss of accuracy in the geometric model. There are two manifestations of diffraction. The first is the difficulty in estimation of the slopes near the edges because of the ringing in the region of the discontinuity of the aperture. This results in inaccurate slope estimates near the edges of the aperture. When the slopes are integrated, the errors incurred in estimation of the wave front are small and localized at the edge. Second, the spatial resolution is limited to the Fresnel length $\sqrt{\lambda z}$, where λ is the wavelength of the light.[6] Figure 4 shows a typical realization of the simulated and reconstructed wave-front slopes and the corresponding wave front. In this example, the length of the linear aperture is 1 m, $z = 5000$ m, and $\lambda = 589$ nm, giving a Fresnel length of 0.054 m. The simulated turbulence obeys Kolmogorov statistics,[11] with Fried's parameter[12] r_0 set to 0.1 m at $\lambda = 589$ nm. It can be seen from Fig. 4(b) that the estimated wave front is smoother than the true wave front.

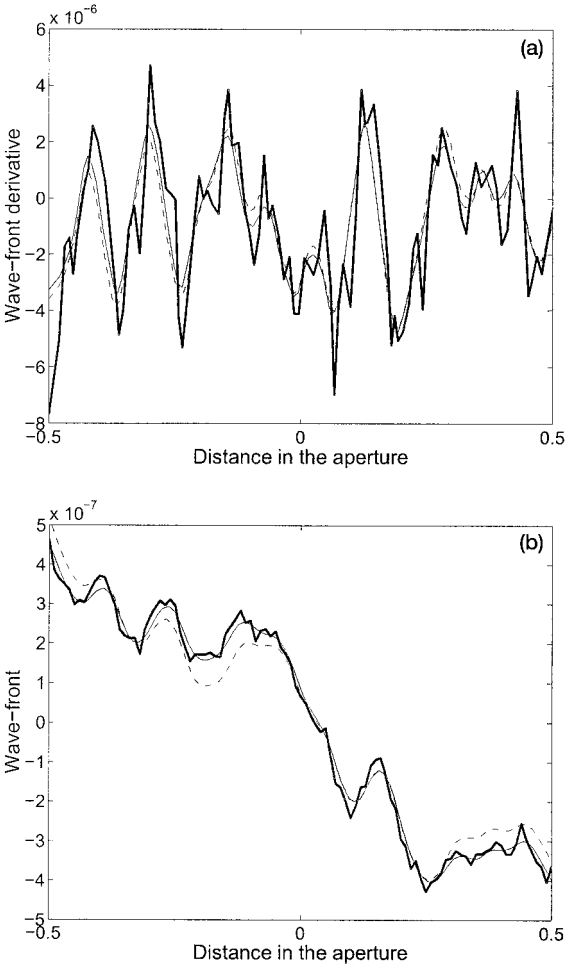

Fig. 4. (a) Wave-front derivative estimates and (b) the wave-front estimates. The thick solid curves, the thin solid curves, and the dashed curves represent the true quantities, the estimates with an infinite light level, and estimates with 10,000 photons on each detector, respectively.

4. Wave-Front Reconstruction in Two Dimensions

We now consider the more complicated two-dimensional case. A circular aperture is treated here for both mathematical convenience and practical significance, but the analysis is valid for an aperture of any shape. In the circular case, Zernike polynomials are a set of orthonormal basis functions that can be used to describe wave-front aberrations:

$$W(x, y) = \sum_{k=1}^{\infty} d_k Z_k, \qquad (18)$$

where d_k is the coefficient of the kth Zernike polynomial Z_k.[13]

It is not possible to match two-dimensional CDFs directly with histogram specification. However, the data can be reduced to one dimension when we form a marginal PDF. The marginal PDF in the x direction is obtained when we take a projection parallel to the y axis of the two-dimensional PDF:

$$f_X(x) = \int_{-\infty}^{\infty} f_{X,Y}(x, y)\mathrm{d}y. \qquad (19)$$

The CDF is then computed when we integrate the marginal PDF in the x direction:

$$C(x) = \int_{-\infty}^{x} f_X(x')\mathrm{d}x'. \qquad (20)$$

A similar expression is obtained for $C(y)$. The ordinates $u_1(i)$ and $u_2(i)$ are found from Eq. (16), and the mean wave-front slopes are then obtained from Eq. (17).

When we use the CDF in two orthogonal directions x and y, only the wave fronts of the form $W(x, y) = \beta(x) + \gamma(y)$, where β and γ are arbitrary functions, can be reconstructed. In terms of Zernike polynomials, this encompasses $Z_2 = 2x$, $Z_3 = 2y$, $Z_4 = \sqrt{12}(x^2 + y^2 - 1)$, and $Z_6 = \sqrt{6}(x^2 - y^2)$ but not $Z_5 = 2\sqrt{6}xy$. However, it is desirable to estimate more Zernike coefficients to obtain a more detailed estimate of the wave front. The solution implemented here is to take projections of the intensity distributions over a range of different angles, not just at 0 and 90 deg. Four projections are required to compute

the first 14 Zernike coefficients, and eight are sufficient for the first 44 coefficients.

The process of rotating a function over a range of angles and taking line integrals through the rotated function is called the Radon transform.[14] The Radon transform of $f_{X,Y}(x, y)$ is denoted as $\mathcal{R}[f_{X,Y}(x, y)]$ or $P(u, \alpha)$ and is given by[14]

$$P(u, \alpha) = \int_L f_{X,Y}(x, y)\mathrm{d}l, \tag{21}$$

where the integral path L is defined by

$$L = [(x, y) : x \cos(\alpha) + y \sin(\alpha) = u]. \tag{22}$$

Hence the Radon transform here consists of rotating $f_{X,Y}(x, y)$ by α degrees, then integrating along the y axis. For example, the Radon transform at $\alpha = 0$ is

$$P(u, 0) = \int_{-\infty}^{\infty} f_{X,Y}(x, y)\mathrm{d}y. \tag{23}$$

In practice, a discrete version of the Radon transform is used, where the integration is replaced by a summation.

To reconstruct the wave front, the Radon transform of the PDFs corresponding to intensity distributions I_1 and I_2 is taken to obtain $P_1(u, \alpha)$ and $P_2(u, \alpha)$. These two quantities are integrated along u to give their respective CDFs, $C_1(u, \alpha)$ and $C_2(u, \alpha)$:

$$C_1(u, \alpha) = \int_{-\infty}^{\infty} P_1(u', \alpha)\mathrm{d}u', \tag{24}$$

with a corresponding equation for $C_2(u, \alpha)$. From these, $u_1(i, \alpha)$ and $u_2(i, \alpha)$ are obtained as before:

$$C_1[u_1(i, \alpha), \alpha] = C_2[u_2(i, \alpha), \alpha] = s(i). \tag{25}$$

These points are used to find the estimates of the mean wave-front slopes in the direction perpendicular to the projections:

$$\left\langle \frac{\partial W\{[u_1(i, \alpha) + u_2(i, \alpha)]/2\}}{r\partial[\cos(\alpha)\hat{x} + \sin(\alpha)\hat{y}]} \right\rangle = \frac{u_1(i, \alpha) - u_2(i, \alpha)}{2z}, \tag{26}$$

where $r = \sqrt{x^2 + y^2}$, and $\hat{x}$ and $\hat{y}$ are the unit vectors in the x and y directions, respectively. The denominator of the left-hand side states that the derivative is taken at right angles to the direction of the projection. For example, if $\alpha = 0$, then one obtains estimates of the mean value of $\partial W/\partial x$ as a function of x, where the mean is taken over all values of y. The location of these mean slope estimates is irregular; however, mean slope estimates at regular intervals, corresponding to the ordinates of the discrete Radon transform, can be obtained by interpolation. For every value of α, a vector of the mean wave-front slopes as a function of integer u values $p_\alpha(u)$ is obtained. These vectors $p_\alpha(u)$ are sufficient to define the wave front to within a piston term; in the algorithm here, the wave front is defined by Zernike coefficients.

For every Zernike polynomial to be fitted, the mean slope of the polynomial in the orthogonal direction to the projection is required. For every angle α, this quantity, denoted as $H_\alpha(u, Z_i)$, is given by

$$H_\alpha(u, Z_i) = \frac{1}{L(u)} \mathcal{R}\left[\frac{\partial Z_i(x, y)}{\partial x} \cos(\alpha) + \frac{\partial Z_i(x, y)}{\partial y} \sin(\alpha), \alpha \right], \tag{27}$$

where $L(u)$ is the length of the integration path. For a circle of radius R,

$$L(u) = 2\sqrt{R^2 - u^2}, \qquad \text{for } u \in [-R, R]. \tag{28}$$

The division by $L(u)$ is necessary to convert the sum of slopes of the Zernike polynomials to mean slopes.

The derivatives of the Zernike polynomials can be computed directly from their mathematical definition.[13] The Zernike coefficients d_i are then found when we least squares fit the data $p_\alpha(u)$ to the model $H_\alpha(u, Z_i)$:

$$d_i = [H_\alpha(u, Z_i)^T H_\alpha(u, Z_i)]^{-1} H_\alpha(u, Z_i)^T p_\alpha(u). \tag{29}$$

The success of this method hinges on the linearity of the Radon transform, which ensures that $p_\alpha(u)$ is a linear function of the wave-front aberration.

5. Simulations

Computer simulations were employed to gauge the performance of this wave-front sensing algorithm. Random phase screens with Kolmogorov statistics were generated by the method of Harding *et al.*[11] The diameter of the circular aperture was 1 m; and Fried's parameter was set to 0.1 m, corresponding to the likely conditions of future experimental research. The wavelength $\lambda = 589$ nm corresponds to the frequency of resonant scattering of the sodium D_2 resonance line. For the purposes of simulating the performance of the algorithm, it is not necessary to simulate the actual experimental setup of the curvature sensor, which includes a converging lens, a variable curvature mirror, and reimaging optics.[15] Instead, it is sufficient to propagate the wave by distances $\pm z$ with the Fresnel propagation formula.[16] In this case, the scaling of the images is unchanged, so the image of the aperture with no wave-front aberration is of the same size as the physical aperture. The detector here consists of a 128×128 array of 1-cm^2 pixels. There were 1000 simulations for each value of z, which varied between 5 and 80 km. After propagation, photon noise with Poisson statistics was added to the intensity distributions. The mean number of photons in each detector was varied between 100 and 10^6. In the simulations, the Radon transform was taken for eight different angles, and the polynomials Z_2 to Z_{21} were fitted. If the number of fitted polynomials is too large, the reconstruction

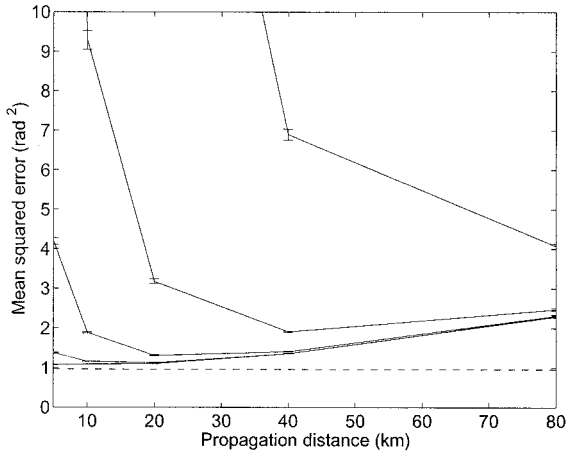

Fig. 5. Simulation results, with σ error bars, of the phase error in the reconstruction of the wave front. The curves represent the mean squared error detecting the following average number of photons at each detector, from top to bottom: 10^2, 10^3, 10^4, 10^5, and 10^6. The dotted line is the theoretical minimum error obtainable if only the first 21 Zernike polynomials are fitted.

from any set of wave-front slope estimates becomes worse, as the high-order coefficients would contain more noise than signal. Truncating the number of fitted polynomials regularizes the reconstruction because it avoids the noise amplification of the high-order terms. A superior approach would be to incorporate prior information in the form of the covariance of the Zernike coefficients to regularize the reconstruction.[17,18] The difficulty with this approach is that the covariance matrix for the noise measurements is also needed. However, the value of this matrix is not yet known for the method proposed in this paper.

The results are plotted in Fig. 5. For comparison, the mean squared phase of the wave front at the aperture is 48 rad^2. As z increases, the sensitivity of the sensor increases at the expense of spatial resolution. The results demonstrate the ability of this algorithm to reconstruct the wave front, even from a small number of photons. It was also verified that this method works even in the presence of strong scintillation in the aperture. We obtained the scintillation by having the turbulent layer 2 km above the aperture and propagating the aberrated wave to the aperture.

The algorithm consists only of matrix multiplications (including the Radon transform and the least-squares reconstruction) and one-dimensional interpolations. Consequently, it is suitable for real-time implementation in an adaptive optics system. Unlike the Shack–Hartmann and curvature sensors, the processing requires the complete images to be available before starting the computation of the wave front. Although this increases the computational demands on the computer hardware, the demands remain within the capacity of existing computing hardware.

6. Conclusion

A novel technique for sensing wave-front aberrations is presented. It is based on the linear relationship between the wave-front slope and the change of the abscissas of the CDF, which is exact in the absence of diffraction. The method is insensitive to scintillation at the aperture and works for polychromatic and extended sources.

Simulation results demonstrate that good reconstructions can be attained down to 100 photons in each detector. In addition, this technique is fast, making it suitable for wave-front sensing in adaptive optics systems.

The authors thank the New Zealand government for financial aid in the form of a Bright Futures scholarship and a Marsden Fund research grant.

References

1. G. Rousset, "Wave-front sensors," in *Adaptive Optics in Astronomy*, F. Roddier, ed. (Cambridge U. Press, Cambridge, UK, 1999), pp. 91–130.
2. J. W. Hardy, *Adaptive Optics for Astronomical Telescopes* (Oxford U. Press, New York 1998), pp. 135–175.
3. R. Ragazzoni, "Pupil plane wave-front sensing with an oscillating prism," J. Mod. Opt. **43,** 289–293 (1996).
4. F. Roddier, "Curvature sensing and compensation: a new concept in adaptive optics," Appl. Opt. **27,** 1223–1225 (1988).
5. W. H. Southwell, "Wave-front estimation from wave-front slope measurements," J. Opt. Soc. Am. **70,** 998–1006 (1980).
6. M. A. van Dam and R. G. Lane, "Extended analysis of curvature sensing," J. Opt. Soc. Am. A **19,** 1390–1397 (2002).
7. J. A. Quiroga, J. A. Gómez-Pedrero, and J. C. Martínez-Antón, "Wavefront measurement by solving the irradiance transport equation for multifocal systems," Opt. Eng. **40,** 2885–2891 (2001).
8. F. Roddier, "Variations on a Hartmann theme," Opt. Eng. **29,** 1239–1242 (1990).
9. M. R. Teague, "Deterministic phase retrieval: a Green's function solution," J. Opt. Soc. Am. **73,** 1434–1441 (1983).
10. R. C. Gonzalez and R. E. Woods, *Digital Image Processing* (Addison-Wesley, Reading, Mass., 1992), pp. 180–181.
11. C. M. Harding, R. A. Johnston, and R. G. Lane, "Fast simulation of a Kolmogorov phase screen," Appl. Opt. **38,** 2161–2170 (1999).
12. F. Roddier, "The effect of atmospheric turbulence in optical astronomy," in *Progress in Optics*, E. Wolf, ed. (North-Holland, Amsterdam, 1981), pp. 283–376.
13. R. J. Noll, "Zernike polynomials and atmospheric turbulence," J. Opt. Soc. Am. **66,** 207–211 (1976).
14. Z.-P. Liang and P. C. Lauterbur, *Principles of Magnetic Resonance Imaging: A Signal Processing Perspective*, Vol. PM76 of the SPIE Press Monographs (SPIE, Bellingham, Wash., 2000), pp. 36–51.
15. F. Roddier, M. Northcott, and J. E. Graves, "A simple low-order adaptive optics system for near-infrared applications," Publ. Astron. Soc. Pac. **103,** 131–149 (1991).
16. J. Goodman, *Introduction to Fourier Optics* (McGraw-Hill, New York, 1996), pp. 63–75.
17. E. P. Wallner, "Optimal wave-front correction using slope measurements," J. Opt. Soc. Am. **73,** 1771–1776 (1983).
18. N. F. Law and R. G. Lane, "Wavefront estimation at low light levels," Opt. Commun. **126,** 19–24 (1996).